Electronic Supplementary Material (ESI) for CrystEngComm.

Supporting Information

for the typescript entitled ”Orthogonal H bonding synthons, actual and virtual structures in molecular crystals: a case study”, by Roberto Centore, Mauro Causa’, Francesca Cerciello, Fabio Capone, Sandra Fusco

1. X-ray molecular structures

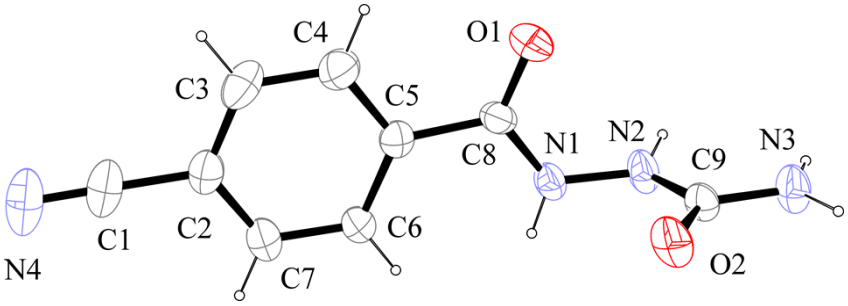

Fig. S1. Ortep diagram of **2**. Thermal ellipsoids are drawn at 30 % probability level.

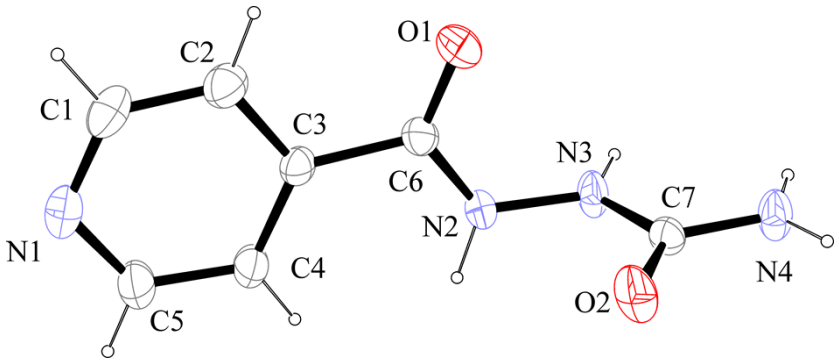

Fig. S2. Ortep diagram of **3**. Thermal ellipsoids are drawn at 30 % probability level.

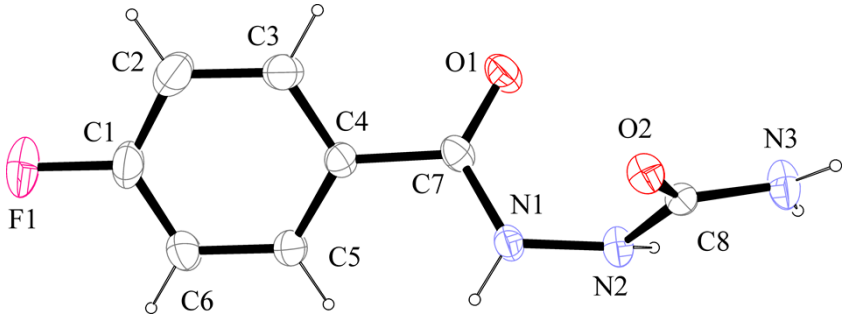

Fig. S3. Ortep diagram of **4**. Thermal ellipsoids are drawn at 30 % probability level.

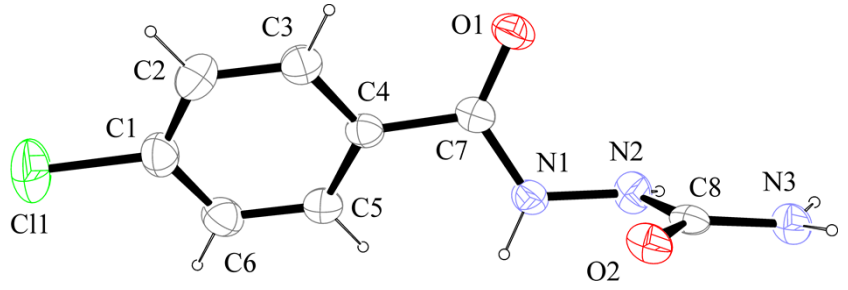

Fig. S4. Ortep diagram of **5**. Thermal ellipsoids are drawn at 30 % probability level.

2. Crystal packing

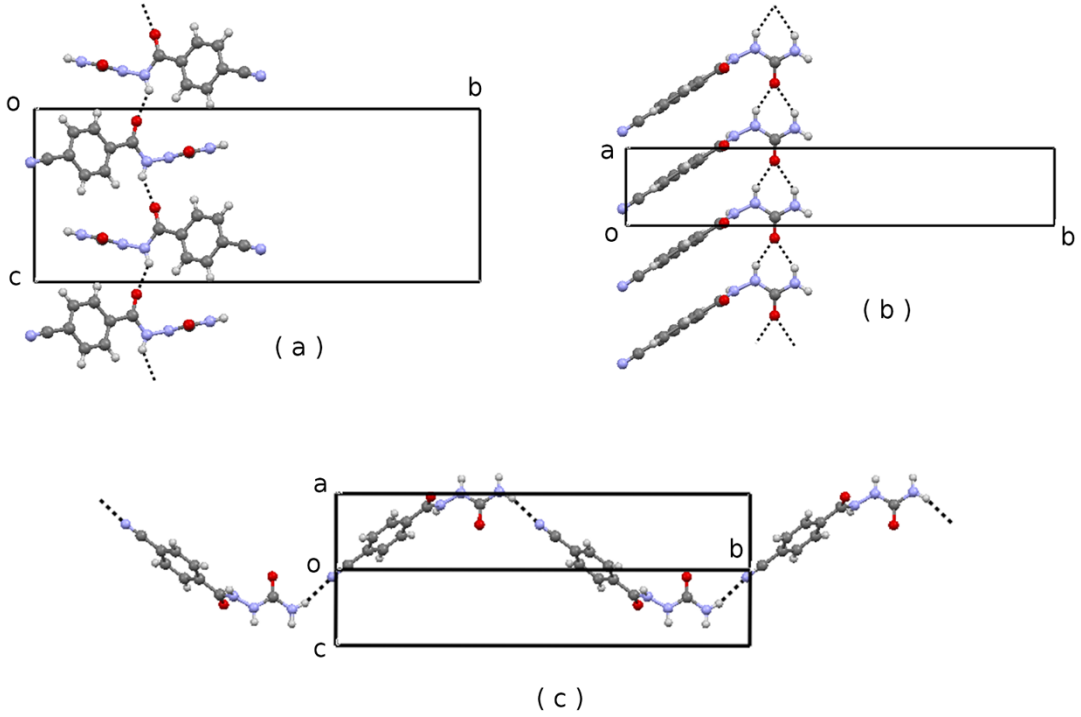

Figure S5. H bonded chains in **2**. (a) Amide-type chain formed by *c*-glide reflection; (b) urea-type chain formed by simple translation. (c) H bonded chain formed between the N–H donor not involved in (a) and (b) patterns and the cyano acceptor; the chain is generated by the 2_1 screw rotation.

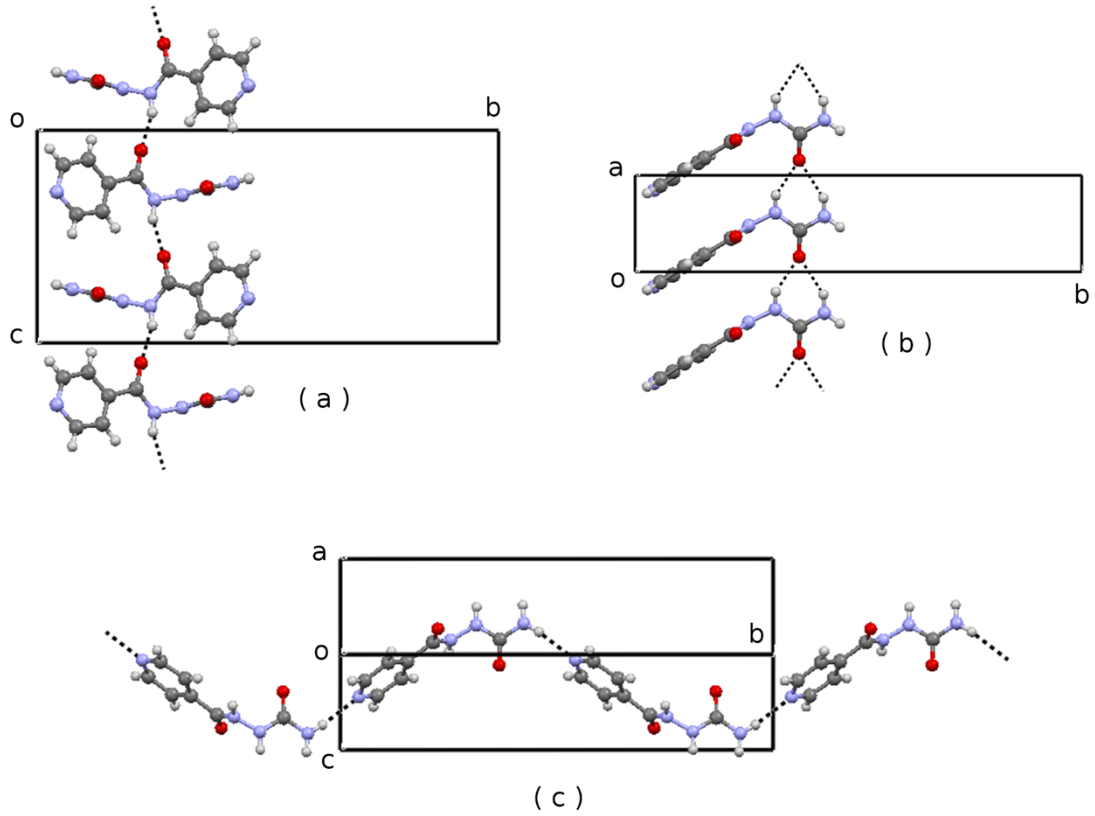

Figure S6. H bonded chains in **3**. (a) Amide-type chain formed by *c*-glide reflection; (b) urea-type chain formed by simple translation. (c) H bonded chain formed between the N–H donor not involved in (a) and (b) patterns and the nitrogen atom acceptor; the chain is generated by the 2_1 screw rotation.

3. Discussion of the X-ray molecular structures

The molecules of the studied compounds have substantially two conformational degrees of freedom: the torsion angle around the phenyl to carbonyl group (*i. e.* C3-C4-C7-N2 for **1**) indicated by ψ, and the torsion angle around the bond N-N (*i. e.* C7-N2-N3-C8 for **1**) indicated by τ. The values of the two torsion angles are gathered in Table S1.

Table S1. Selected torsion angles (°) of the studied compounds.

	1	**2**	**3**	**4**	**5**
ψ	169.4(2)	-175.5(5)	-176.11(16)	145.9(3)	153.8(2)
τ	85.4(2)	85.7(6)	86.5(2)	73.7(4)	95.6(2)

In particular, we note that the torsion of the carbonyl group around the bond with phenyl is increased in the two structures **4** and **5**, as compared with the structures of semicarbazides **1**, **2** and **3** which are isomorphous to each other.

4. Geometric data of hydrogen bonds in the X-ray structures

The geometric parameters of the hydrogen bond D–H···A are given in the following order: D–H (Å), H···A (Å), D···A (Å), D–H···A (°), symmetry code of the acceptor atom.

Table S2. H-bonding geometry in **1**, **2** and **3**.

	D–H···A	D–H	H···A	D···A	D–H···A	Symmetry code of A
1	N2–H···O1	0.88(2)	1.95(2)	2.785(3)	158(2)	x, 1/2-y, -1/2+z
	N4–H···O3	0.87(2)	2.64(3)	3.302(4)	134(2)	2-x, -1/2+y, 1/2-z
	N4–H···O4	0.87(2)	2.47(2)	3.332(3)	175(2)	2-x, -1/2+y, 1/2-z
	N3–H···O2	0.86(2)	2.06(2)	2.830(3)	147(2)	-1+x, y, z
	N4–H···O2	0.90(3)	2.01(3)	2.811(3)	148(2)	-1+x, y, z
2	N1–H···O1	0.84(6)	2.00(6)	2.794(7)	157(5)	x, 1/2-y, -1/2+z
	N3–H···N4	0.91(7)	2.24(7)	3.124(8)	165(6)	-x, 1/2 + y, 1.5-z
	N2–H···O2	0.81(7)	2.09(7)	2.806(6)	147(6)	1 + x, y, z
	N3–H···O2	0.80(8)	2.11(8)	2.838(6)	152(7)	1 + x, y, z
3	N1–H···O1	0.91(2)	1.91(2)	2.789(3)	160(2)	x, 1/2-y, -1/2+z
	N4–H···N1	0.84(2)	2.17(2)	2.999(2)	169(2)	-x, -1/2+y, 1/2-z
	N3–H···O2	0.84(2)	2.04(2)	2.796(2)	149(2)	1 + x, y, z
	N4–H···O2	0.87(2)	2.03(2)	2.823(3)	151(2)	1 + x, y, z

Table S3. Geometry of H bonding and intermolecular contacts in **4** and **5**.

	D–H···A	D–H	H···A	D···A	D–H···A	Symmetry code of A
4	N1–H···O2	0.85(4)	2.04(4)	2.862(3)	162(4)	-x, -y, 1- z
	N3–H···O2	0.85(5)	2.13(4)	2.962(4)	163(4)	-1-x, -y, 1-z
	N2–H···O1	0.97(4)	1.91(4)	2.864(4)	167(4)	x, 1/2-y, 1/2+z
	N3–H···O1	0.79(4)	2.46(4)	3.164(5)	149(4)	x, 1/2-y, 1/2+z
	N3–H···F	0.85(5)	2.61(4)	2.938(5)	104(3)	-1+x, y, 1+z
5	N1–H···O2	0.84(3)	2.07(3)	2.881(3)	162(2)	-x, -y, -z
	N3–H···O1	0.84(2)	2.28(2)	3.062(3)	155(2)	-1-x, -y, -z
	N2–H···O2	0.84(3)	1.96(3)	2.760(3)	161(2)	x, -1+y, z
	N3–H···O2	0.83(3)	2.50(3)	3.110(3)	132(2)	x, -1+y, z
	N3–H···O1	0.83(3)	2.43(2)	3.098(3)	138(2)	-1-x, -1-y, -z

We have considered, in particular, the contact N3–H···F present in **4** (see table S3 and Fig. 4(b) of the typescript). The H···F distance reported in Table S4, 2.61(4) Å, is not significantly different from the sum of the van der Waals radii of hydrogen and fluorine (1.20 Å + 1.47 Å = 2.67 Å). If the N–H bond is normalized (see ref. 26 of the typescript), the structural parameters of the N3–H···F contact become 1.002, 2.575, 2.938, 101°, so the H···F distance is only 0.1 Å shorter than the sum of van der Waals radii. This indicates that the contact N3–H···F has to be considered basically a van der Waals contact and not a H bond.

5. Definition and calculation of lattice energies

We define the lattice formation energy U_{lat} as the difference between the DFT molar energy of the crystal (E_{cry}) and the DFT molar energy of the free molecules (E_{mol}):

$$U_{lat} = E_{cry} - E_{mol}$$

We have estimated the Gibbs free energy of the lattice formation, G^o_{lat}, at room temperature and pressure (T^0 = 298 K, P^0 = 10^5 Pa) as the difference between the molar Gibbs free energy of the crystal (G^o_{cry}) and the molar Gibbs free energy of the isolated molecules (G^o_{mol}).

$$G^o_{lat} = G^o_{cry} - G^o_{mol}$$

The molar Gibbs free energy of the crystal G^o_{cry} is estimated as the sum of the molar DFT energy of the crystal E_{cry}, the vibrational zero point molar energy of the crystal $E_{0,vib}$, the vibrational molar energy of the crystal at room temperature $E_{vibcry}(T^0)$, the enthalpic term and the vibrational molar entropic term $-T^0 S_{vibcry}$.

$$G^0_{cry} = E_{cry} + E_{0,vibcry} + E_{vibcry}(T^0) - T^0 S_{vibcry}(T^0)$$

The vibrational dynamical problem of the lattice is studied within the harmonic approximation, from the numerical derivatives of the analytical gradient of the Born-Oppenheimer potential energy surface.[1] The optical phonons are calculated only in the Γ point of the reciprocal space: this approximation is very good for molecular crystals like those described in the present study.[2]

The molar Gibbs free energy of the isolated molecules, G^0_{mol}, is calculated as the molar Gibbs free energy of an ideal gas. The DFT molar energy of the isolated molecules, E_{mol}, is summed to the molar zero point vibrational energy of the isolated molecules $E_{0,vib}$, to the rotational $E_{rot}(T^0)$ and vibrational $E_{vib}(T^0)$ molar energies of the isolated molecules at room temperature, to the enthalpic

term RT^0 and to the rotational and vibrational entropic terms $-T(S_{rot}+S_{vib})$. The vibrational terms are calculated within the harmonic approximation, and the rotational terms are calculated treating the molecule as a rigid asymmetric top, following a consolidated procedure in molecular quantum chemistry.[3]

$$G^0_{mol} = E_{mol} + E_{0,vib} + E_{rot}(T^0) + E_{vib}(T^0) + RT^0 - T^0(S_{rot}(T^0) + S_{vib}(T^0))$$

The lattice vibrational analysis produced the vibrational eigenvalues and eigenvectors of the hessian matrix in the Γ point (the center of the Brillouin zone). The eigenvalues represent the second derivative of the electronic energy with respect to the 3N-3 optical normal modes. The positive sign of all the 3N-3 eigenvalues is the necessary and sufficient condition for the existence of a local minimum. For all the structures corresponding to the supposed *U*ij minima, we got 3N-3 positive Hessian eigenvalues, and this allows us to define them as true minima. The other 3 eigenvalues, corresponding to the translational modes of the 3D model, are computationally zero, because correspond to the acoustic vibrational modes, whose frequency vanishes in the Γ point.

References

[1] F. Pascale, C. M. Zicovich-Wilson, F. Lopez Gejo, B. Civalleri, R. Orlando and R. Dovesi, ``The calculation of vibrational frequencies of crystalline compounds and its implementation in the CRYSTAL code", *J. Comput. Chem.*, 2004, **25**, 888-897.

[2] S. Tosoni, F. Pascale, P. Ugliengo, R. Orlando, V. R. Saunders and R. Dovesi, ”Quantum mechanical calculation of the OH vibrational frequency in crystalline solids", *Mol. Phys.*, 2005, **103**, 2549-2558.

[3] D. A. McQuarrie and J. D. Simon, *Molecular Thermodynamics*, 1999, University Science Books, Sausalito (CA, USA).

6. Optimization procedure and results

Each structure was first optimized in its own packing, starting from the corresponding room temperature (RT) crystal structure (cell and fractional coordinates). In this way, the lattice energies U_{11}, U_{21}, U_{31}, U_{42}, U_{53} (and the corresponding lattice densities, entropies and Gibbs free energies) were obtained. For the optimization of the semicarbazides in the packings of other semicarbazides, the procedure was as follows.

For the optimizations in packing type 1, the initial model was assembled starting from the RT crystal structure of **1** (cell and fractional coordinates) replacing the nitro group by a fluorine (U_{41}) or chlorine atom (U_{51}). Standard values for the bond lengths and angles were considered.

For the optimizations in packing type 2, the initial model was assembled from the RT crystal structure of **4** (cell and fractional coordinates) replacing the fluorine atom by a nitro group (U_{12}), cyano group (U_{22}), *para*-nitrogen atom (U_{32}) or chlorine atom (U_{52}), using standard values for the bond lengths and angles.

For the optimizations in packing type 3, the initial model was assembled from the RT crystal structure of **5** (cell and fractional coordinates) replacing the chlorine atom by a nitro group (U_{13}), cyano group (U_{23}), *para*-nitrogen atom (U_{33}) or fluorine atom (U_{43}), using standard values for the bond lengths and angles.

In Table S4 we report the experimental cell parameters at 298 K and 173 K and the optimized cell parameters for all the semicarbazides.

Table S4. Experimental cell parameters at 298 K, 173 K and optimized cell parameters for **1**, **2**, **3**, **4** and **5**.

Compound	*a* (Å)	*b* (Å)	*c* (Å)	*β* (°)
1 (298 K)	4.524(3)	23.583(7)	9.537(4)	108.39(2)
1 (173 K)	4.520(1)	23.299(5)	9.462(3)	109.085(4)
1 opt	4.4886	22.6455	9.3497	111.97
2 (298 K)	4.508(2)	24.110(8)	9.612(4)	105.38(2)
2 (173 K)	4.503(2)	23.903(6)	9.554(3)	107.44(2)
2 opt	4.4846	23.3489	9.3686	111.420
3 (298 K)	4.513(2)	20.038(7)	9.619(5)	106.34(2)
3 (173 K)	4.515(2)	19.982(7)	9.555(5)	108.75(2)
3 opt	4.5104	19.8942	9.4009	114.64
4 (298 K)	7.785(4)	13.578(6)	8.459(4)	99.74(2)

4 173 (K)	7.746(4)	13.458(6)	8.415(4)	99.51(2)
4 opt	7.7535	13.0315	8.3428	100.87
5 (298 K)	6.786(4)	4.604(3)	30.169(8)	90.76(3)
5 (173 K)	6.733(4)	4.583(3)	30.058(6)	90.68(3)
5 opt	6.4898	4.5509	30.1063	89.31

In Table S5 we report the cell parameters for the optimized structures. Each structure is identified in the first column by a two-number code, mn. The first number identifies the compound (Chart 1 of the typescript, m = 1, 2, 3, 4, 5), the second identifies the type of packing (n = 1, 2, 3).

Table S5. Cell parameters for the optimized structures. The cell parameters of the optimized structures corresponding to the real structures (also given in Table S4) are highlighted in yellow.

Structure	*a* (Å)	*b* (Å)	*c* (Å)	*β* (°)
11	4.4886	22.6455	9.3497	111.97
12	7.5278	13.4644	8.9100	105.07
13	6.4805	4.5675	30.1430	93.63
21	4.4846	23.3489	9.3686	111.420
22	7.8226	13.3713	8.9299	105.67
23	6.2822	4.5454	31.3637	93.13
31	4.5104	19.8942	9.4009	114.64
32	7.40531	13.8431	7.8201	91.39
33	6.2273	4.5987	27.4056	99.94
41	4.5026	19.4527	9.4888	104.70
42	7.7535	13.0315	8.3428	100.87
43	6.4284	4.5501	28.6564	86.73
51	4.5142	23.0919	9.4181	111.82
52	7.7008	13.5214	8.9511	106.71
53	6.4898	4.5509	30.1063	89.31

Considering the real structures, Table S4, the agreement between the lattice parameters of the room temperature X-ray structures and those of the optimized structures is quite good. The agreement between cell axes is within 4 % and between angles is within 8 %. The figures drop to 3 % and 5 % if the experimental lattice parameters measured at 173 K are considered. The good agreement between the experimental and optimized lattice parameters is indicative of the soundness of the theoretical method used in the calculations and of the reliability of the estimated theoretical quantities (lattice energy, density etc.).

In the case of the virtual structures, of course we do not have any experimental datum to be compared with. However, a useful comparison can be performed between the final optimized lattice parameters of the virtual structure and the lattice parameters of the actual (experimental) structure from which the starting model is built up (*vide supra*). This is shown in Table S6.

Table S6. Variation of each optimized lattice parameter as compared with the initial model for the virtual structures.

Virtual structure	$\Delta a/a$	$\Delta b/b$	$\Delta c/c$	$\Delta\beta/\beta$
41	-0.4 %	-16 %	0.3 %	-4 %
51	-0.1 %	-0.9 %	-0.4 %	2 %
12	-3 %	0.05 %	6 %	5 %
22	1 %	-0.6 %	6 %	6 %
32	-4 %	3 %	-7 %	-8 %
52	-0.6 %	0.5 %	6 %	7 %
13	-4 %	-0.8 %	-0.1 %	3 %
23	-7 %	-1 %	4 %	3 %
33	-8 %	-0.1 %	-9 %	10 %
53	-5 %	-1 %	-5 %	-4 %

Also in this case the changes due to the optimization procedure are rather small, that indicating that the experimental packing of a specific semicarbazide is a good starting model for the packing of every other. The most relevant change is observed for the *b* axis of the virtual structure 41. But this is clearly expected because, in the packing of type 1, the *b* axis is related with the length of the molecule and the starting model for the optimization is that of semicarbazide **1**, which has a molecular length significantly higher than **4** (nitro group instead of fluorine atom). In summary, the data of Table S6 clearly confirm the virtual isomorphism of all the investigated semicarbazides in each of the three packings. This is also confirmed by the structural parameters ψ and τ (*vide supra*) of the optimized structures (Table S7), which keep similar values for different semicarbazides optimized in the same packing.

Table S7. Selected torsion angles (°) of the optimized structures. The optimized structures corresponding to the real structures are highlighted in yellow.

Structure	ψ (°)	τ (°)
11	168.83	-82.62
12	130.78	63.82
13	152.79	92.27
21	170.28	-86.12
22	134.20	66.70
23	151.85	94.69
31	-168.61	85.62
32	130.97	61.52
33	150.81	92.27
41	-176.18	-92.52
42	146.60	73.34
43	152.09	92.84
51	167.43	-83.90
52	146.15	70.90
53	152.51	93.28

Table S8. Matrix of the lattice entropy for the optimized crystal structures at 298 K (values in cal/(Kmol)).

S_{11}= -59.75	S_{12}= -63.93	S_{13}= -61.27
S_{21}= -61.93	S_{22}= -65.21	S_{23}= -63.14
S_{31}= -61.32	S_{32}= -62.70	S_{33}= -59.82
S_{41}= -57.85	S_{42}= -58.54	S_{43}= -60.15
S_{51}= -57.30	S_{52}= -60.54	S_{53}= -59.84
S_{61}= -61.23	S_{62}= -62.23	S_{63}= -61.67

7. Discussion of basis sets

In Table S9 the lattice Gibbs free energies already reported in the typescript (Table 3) are given as the difference with respect to the lattice Gibbs free energy calculated for the experimental packing of each compound.

Table S9. G_{lat}^{0} (kcal/mol), base 6-31**, B3LYP, relative to the experimental structure

	1	**2**	**3**	**4**	**5**
Packing 1	0.00	0.00	0.00	3.42	2.91
Packing 2	0.21	-0.05	0.45	0.00	0.60
Packing 3	2.46	1.71	2.55	2.50	0.00

The effect of the basis set has been studied on a subset of data, in particular on semicarbazide **1** in the three different packings. We have used the following basis sets:

- double zeta 6-31G**, already referenced;

- triple zeta "pob".[1]

The data calculated with the triple zeta basis set are given in Table S10.

Table S10, G_{lat}^{0} (kcal/mol), base triple zeta pob BSSE corrected, relative to the experimental structure

	1
Packing 1	0.00
Packing 2	0.71
Packing 3	2.92

By comparing Table S10 with the first column of Table S9, it is clearly shown that the relative free energies calculated with the triple zeta basis set are close to those calculated with the double zeta 6-31G** basis set.

Reference

[1] M. F. Peintinger, D. Vilela Oliveira and T. Bredow, "Consistent Gaussian Basis Sets of Triple-Zeta Valence with Polarization Quality for Solid-State Calculations", *Journal of Computational Chemistry*, 2012, **34**, 451-459.

8. Experimental (bulk) and calculated (from the single crystal data) X-ray diffraction patterns

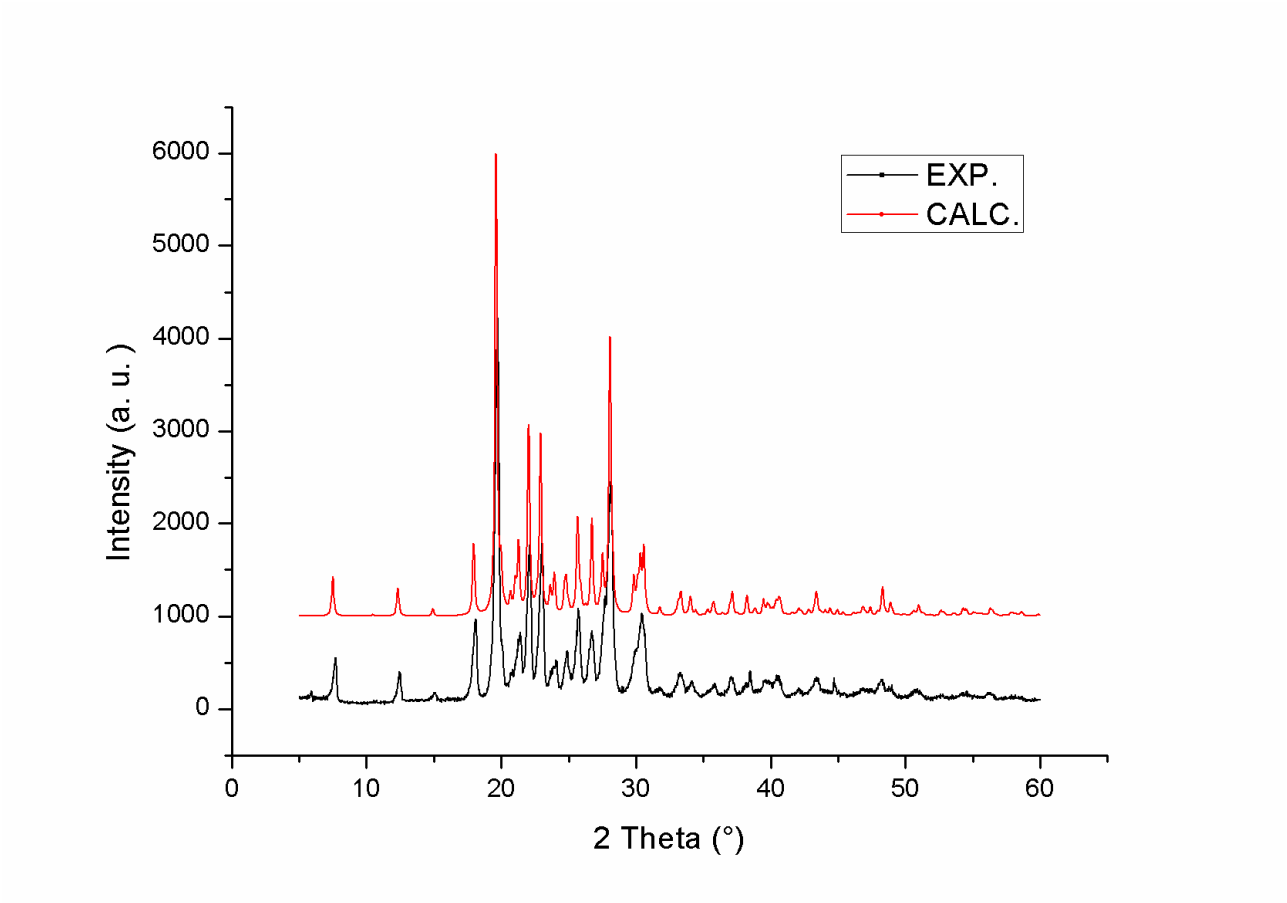

Fig. S7. Experimental (bulk sample, black line) and calculated (from the single crystal structure, red line) X-ray powder diffraction patterns of **1**. CuKα radiation. The red line has been moved upward for clarity.

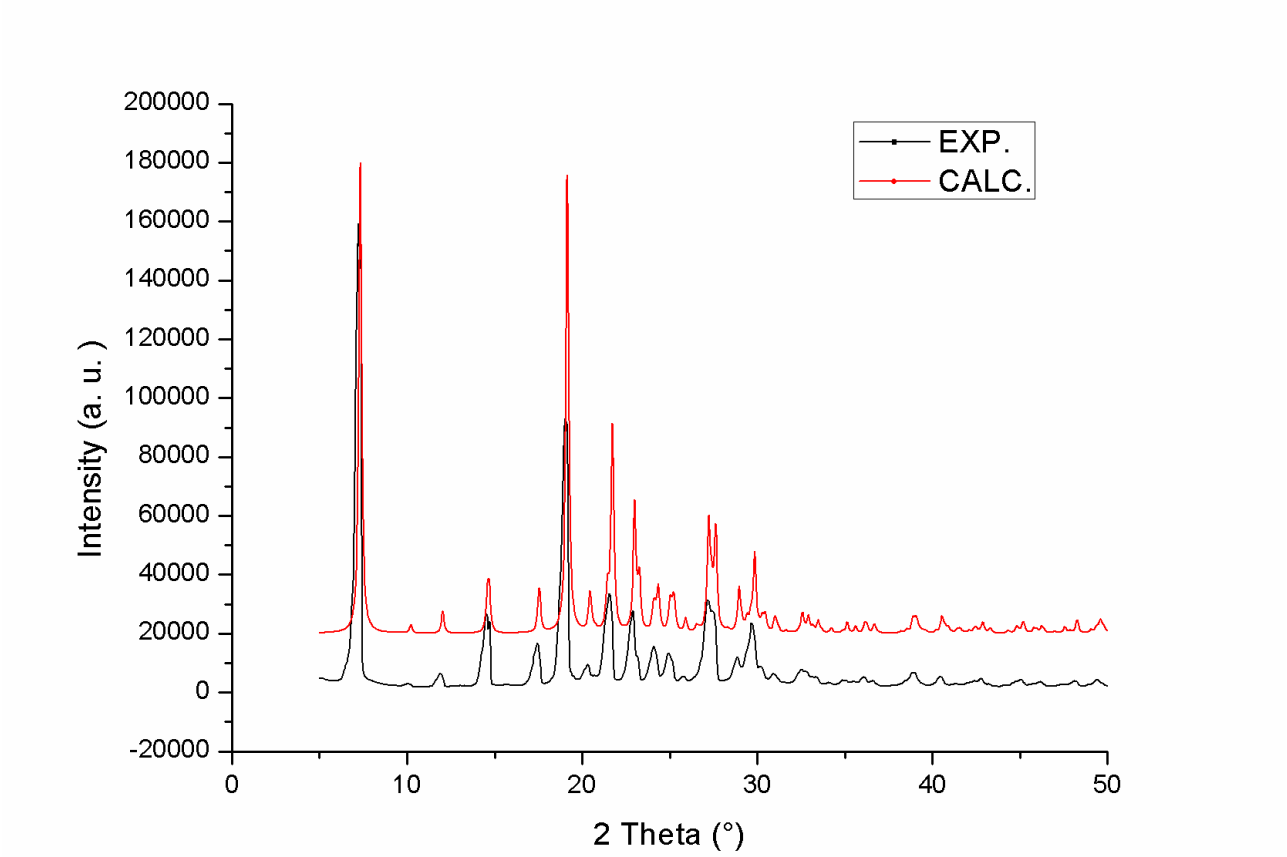

Fig. S8. Experimental (bulk sample, black line) and calculated (from the single crystal structure, red line) X-ray powder diffraction patterns of **2**. CuKα radiation. The red line has been moved upward for clarity.

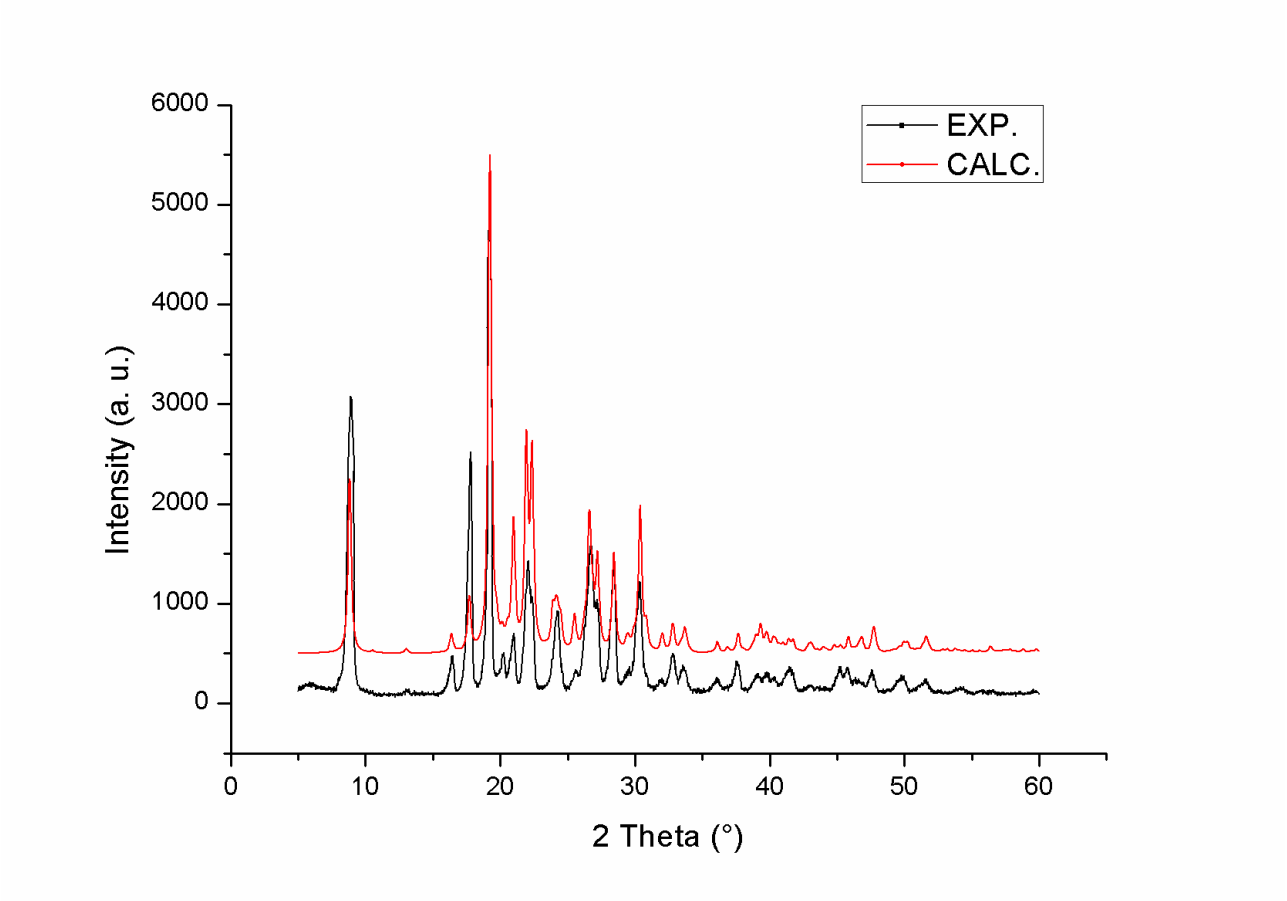

Fig. S9. Experimental (bulk sample, black line) and calculated (from the single crystal structure, red line) X-ray powder diffraction patterns of **3**. CuKα radiation. The red line has been moved upward for clarity.

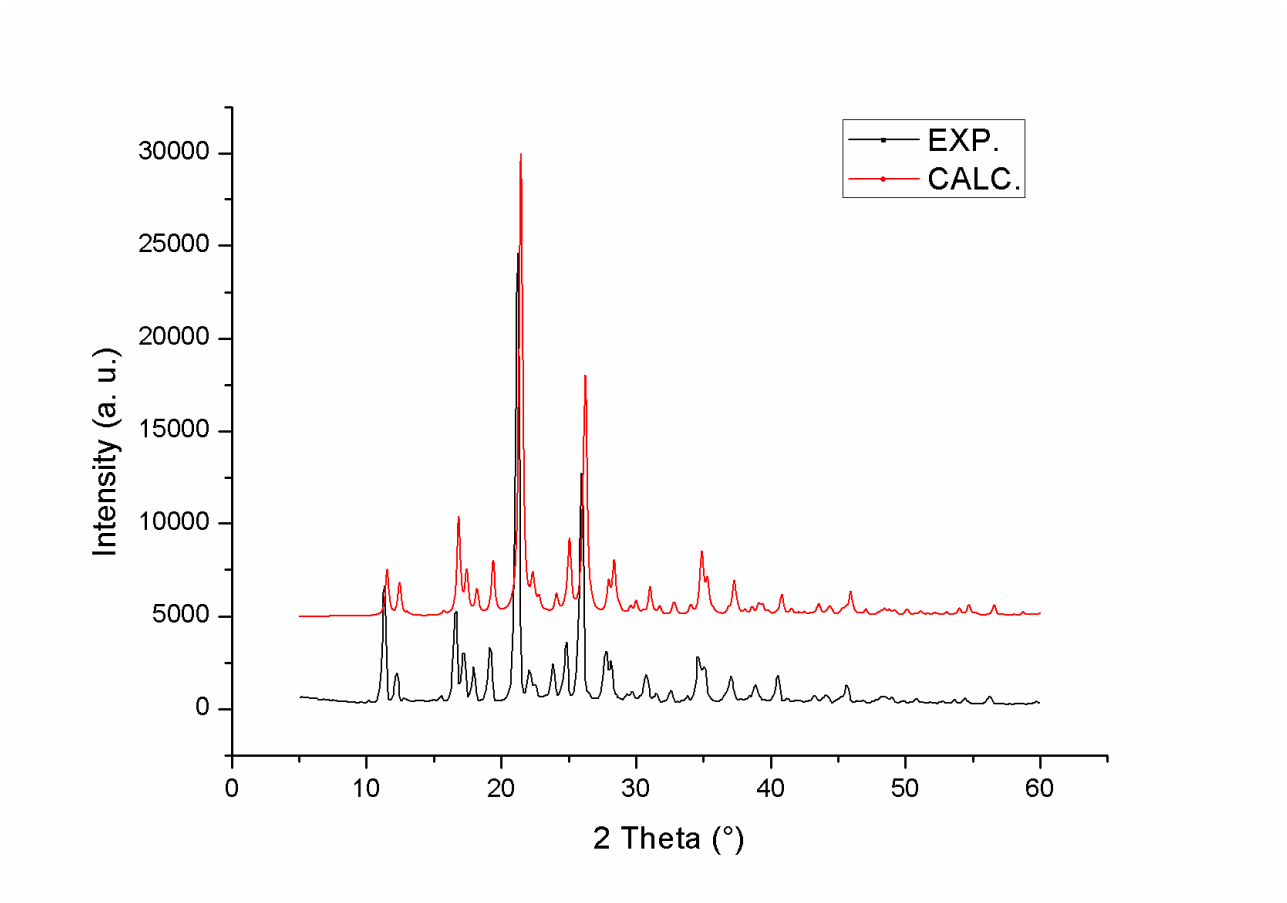

Fig. S10. Experimental (bulk sample, black line) and calculated (from the single crystal structure, red line) X-ray powder diffraction patterns of **4**. CuKα radiation. The red line has been moved upward for clarity.

9. Crystal structure analysis of a different polymorph of semicarbazide 5.

In the case of semicarbazide **5**, slow evaporation of ethanol solutions produces single crystal specimens of different morphology in the same crystallization batch: elongated prisms and large plates, Fig. S11. Optical observations at the polarizing microscope, on heating and cooling, of manually selected single crystals indicate that the elongated prisms (polymorph I) melt at 228 °C (with decomposition), while the large plates (polymorph II) undergo an irreversible solid-solid transition at 198 °C with conversion into polymorph I.

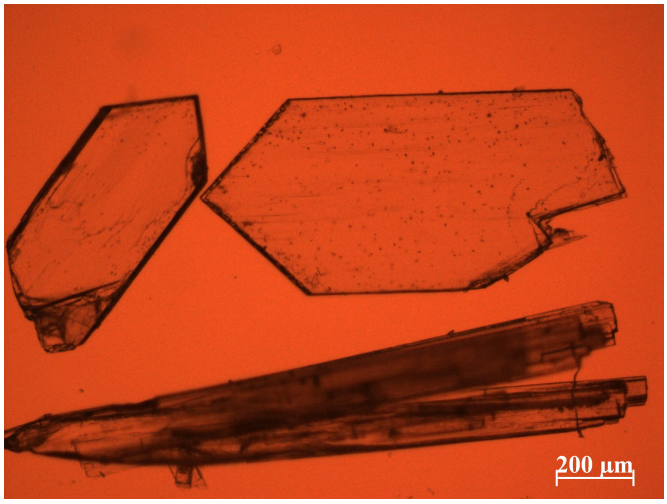

Fig. S11. Single crystals of the two polymorphs of **5**. The crystals were obtained in the same crystallization batch. The elongated prisms at the bottom correspond to the thermodynamically more stable phase described in the typescript (polymorph I), the large plates to the phase described in the present paragraph (polymorph II).

The crystal structure of the thermodynamically more stable polymorph I has been described in the typescript. Here follows the description of the crystal structure of polymorph II (see Table S11). ORTEP diagrams of the independent unit of polymorph II are shown in Figures S12 and S13. The structure shows a relevant degree of static positional disorder. The independent molecule is split in two different positions with complete superposition of the four non-H atoms of the terminal $NHCONH_2$ group.

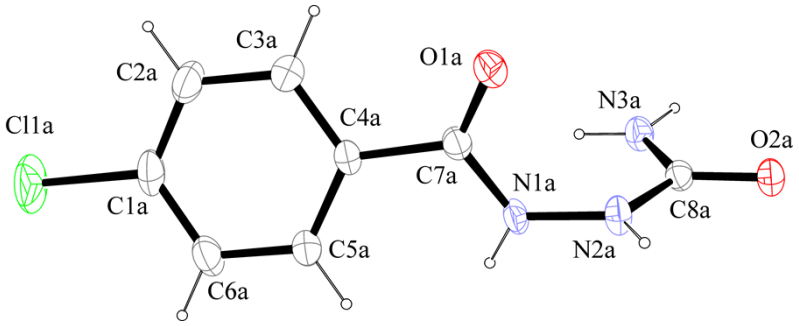

Fig. S12. ORTEP drawing of the molecular structure of **5** in polymorph II. Only the most populated split position is shown. Thermal ellipsoids are drawn at 30 % probability level.

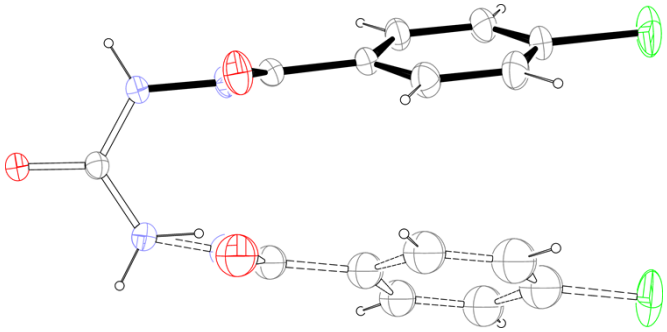

Fig. S13. The two split positions of the independent molecule in polymorph II. The less populated position is dashed. The common bonds are drawn in open style. For the common fragment, only H atoms of the more populated position are shown.

The two split positions, that are clearly related by a non-crystallographic mirror symmetry, have different occupation factors that converged to the final refined values 0.877(3) and 0.123(3). The most relevant feature of the molecular structure is the conformation around the bond N2–C8, that is *s-trans* (N1A-N2A-C8A-N3A=2.9(3)°), while it is *s-cis* in polymorph I (N1-N2-C8-N3= 172.9(2)°, see Fig. S4), as well as in the crystal structures of all the other semicarbazides reported in the typescript.[1] This results in a scorpion tail shape of the molecule (Fig. S14).

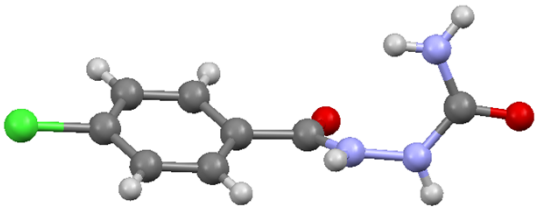

Fig. S14. Ball and stick view of the independent molecule of polymorph II of **5**.

The different conformation of the terminal $CONH_2$ group induces a completely different pattern of H bonds, mainly for the reason that the urea-type synthon is no longer possible. Some features of the crystal packing are shown in Figs. S15 and S16.

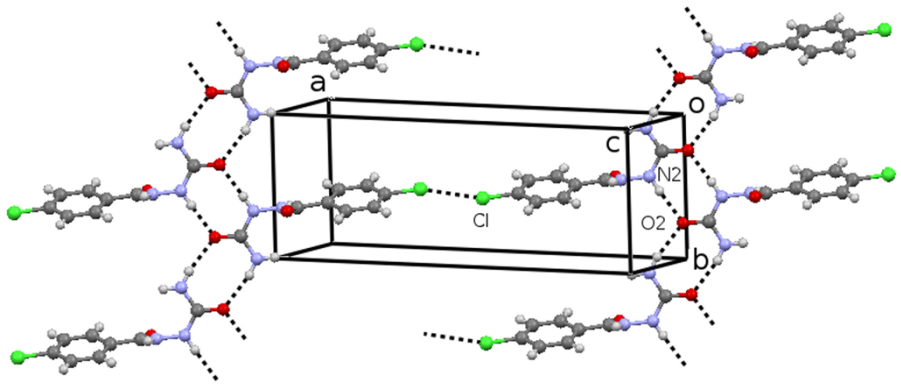

Fig. S15. Partial crystal packing of polymorph II. Only the most abundant split position is shown.

Dimeric ring patterns $R_2^2(8)$ are formed between one urea N–H donor and the urea carbonyl acceptor of centrosymmetrically related molecules (N2A–H···O2A^{i}: 0.860, 1.958, 2.816(3) Å, 174.2°, i = -x, 1-y, -z; N3A–H···O2A^{ii}: 0.860, 2.064, 2.908(3) Å, 166.7°, ii = -x, -y, -z;). The carbonyl is actually bifurcated acceptor and chains of ring patterns are formed that run parallel to the **b** axis (Fig. S15). Adjacent chains are linked by type I chloro-chloro interactions[2] (Cl1A···Cl1a^{ii} = 3.456(2) Å, C1A–Cl1A···Cl1a^{ii} = 152.0(1)°, ii = 1-x, 1-y, 2-z).

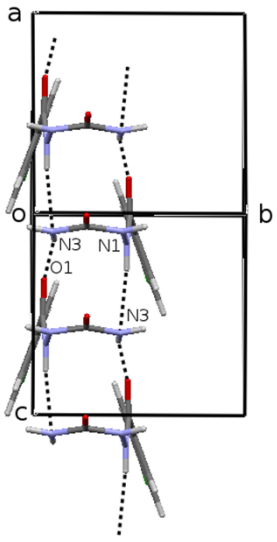

Fig. S16. Partial crystal packing of polymorph II. Only the most abundant split position is shown.

Ring patterns $R_2^2(12)$ are formed involving one urea N–H donor and the amide carbonyl acceptor and the amide N–H donor and the urea N acceptor of a glide related molecule (N3A–H···O1A^{i}: 0.860, 2.210, 3.017(3) Å, 156.4°, i = x, 1/2-y, 1/2+z; N1A–H···N3A^{i}: 0.860, 2.288, 3.031(3) Å, 144.8°, i = x, 1/2-y, 1/2+z). The ring patterns are arranged in chains running parallel to **c** and generated by the *c*-glide operation.

Of course, the concomitant crystallization of both polymorphs in the same batch, see Fig. S11, indicates that both isomers (*s-cis* and *s-trans*) are present in solution.

A comparison of the energy of this packing with the other packings described in the typescript is difficult because of the static disorder and the associated configurational entropy that contributes to the reduction of the free energy. This is why no theoretical computation has been performed for this structure.

Table S11. Crystal collection and refinement data for polymorph II of **5**.

	5 polymorph II
Empirical Formula	$C_8\ H_8\ N_3\ O_2\ Cl$
M	213.62
Space Group	$P2_1/c$
a /Å	20.299(7)
b / Å	6.988(4)
c / Å	6.747(3)
β /°	99.20(4)
V /Å^3	944.7(8)
Z, T /K	4, 293
ρ_{calc} /g·cm^{-3}	1.502
Reflns collected	10010
Unique reflections (R_{int})	2155 (0.0645)
Refined param. (restraints)	173 (32)
R1 [I > 2σ(I)]	0.0577
wR2 [all data]	0.1363
Max. peak/hole (e·Å^{-3})	0.239/-0.232

References

[1] While the *s-trans* conformation found in polymorph II is rare in *N*-substituted ureas, it is relatively frequent in thioureas and thiosemicarbazides. See, as an example, the crystal structure of

N-benzoyl-thiosemicarbazide: H.-D. Bian, G.-Q. Guo, Q. Yu, H. Liang, X.-E. Yang and L.-G. Zhu, *Acta Crystallogr.*, 2005, **E61**, o639-o640.

[2] (a) G. R. Desiraju and R. Parthasarathy, *J. Am. Chem. Soc.*, 1989, **111**, 8725-8726. (b) B. Saha, A. Nangia and J.-F. Nicoud, *Cryst. Growth Des.*, 2006, **6**, 1278-1281.

10. ^{1}H-NMR spectra of the compounds

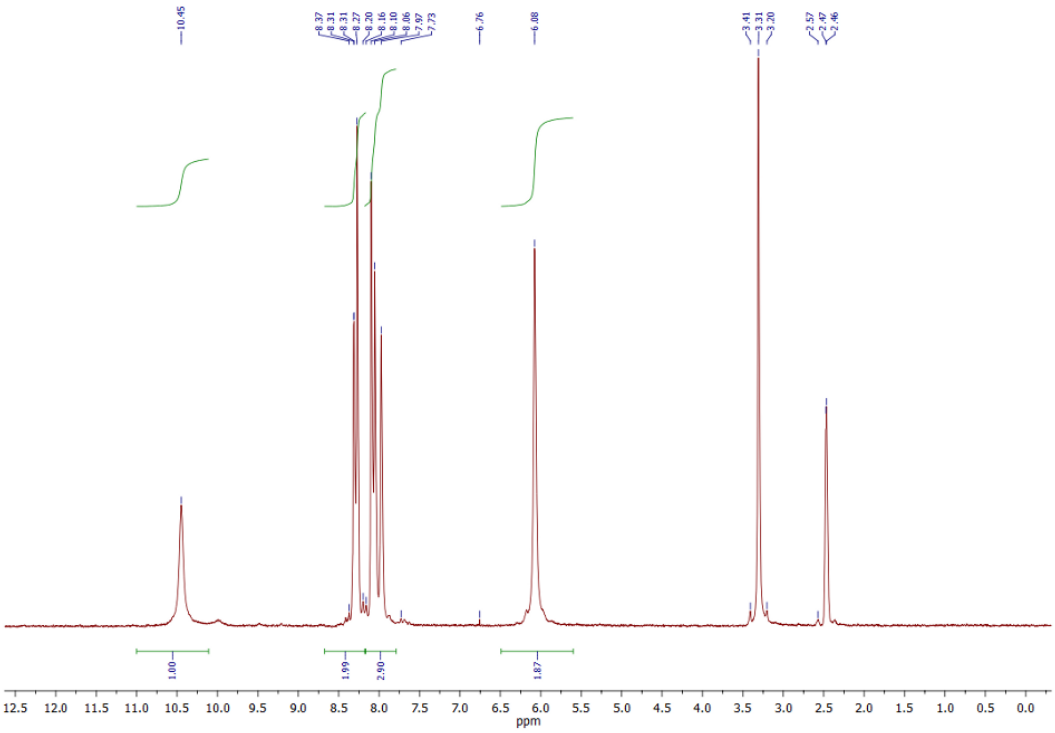

Fig. S17. ^{1}H-NMR spectrum of **1**. Solvent is D6-DMSO.

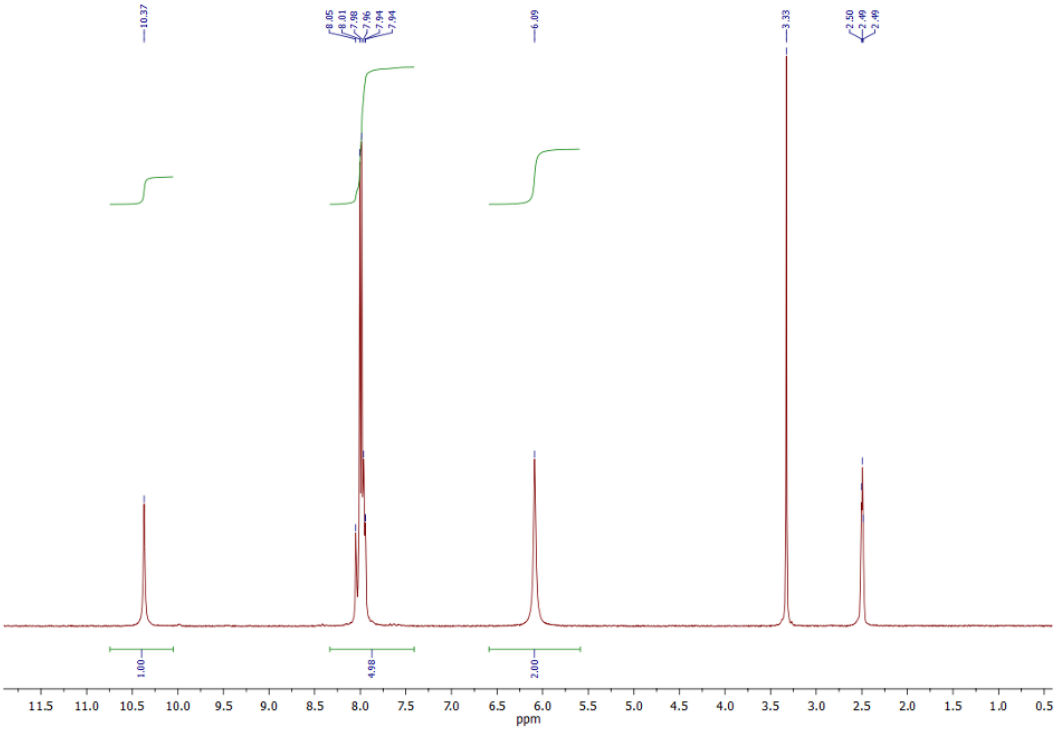

Fig. S18. ^{1}H-NMR spectrum of **2**. Solvent is D6-DMSO.

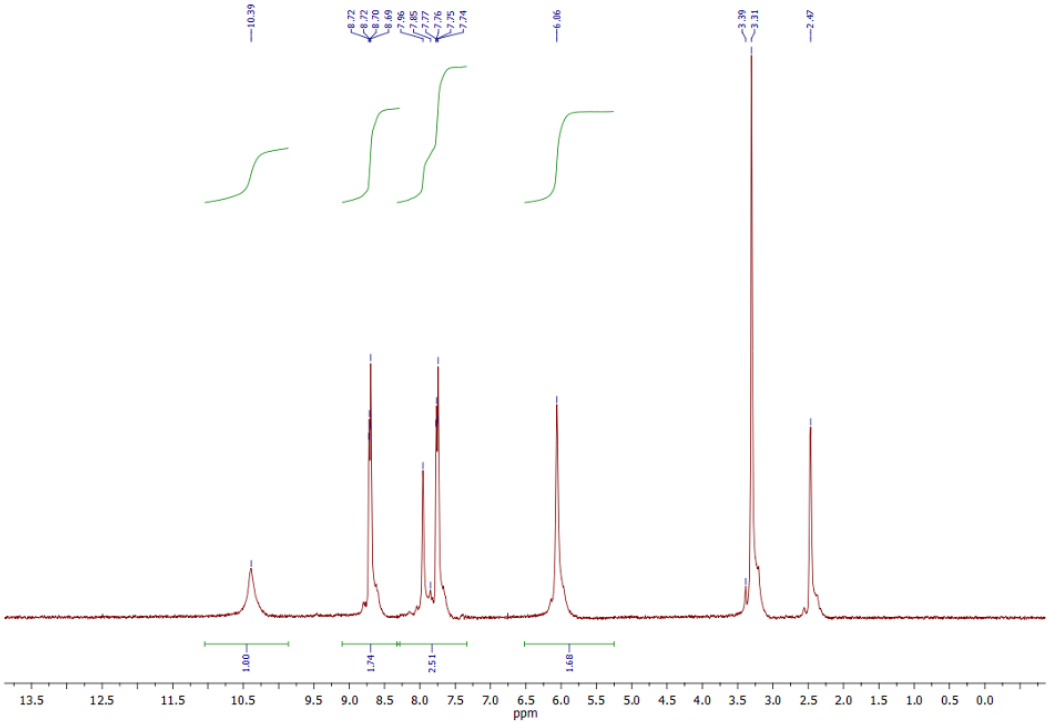

Fig. S19. ^{1}H-NMR spectrum of **3**. Solvent is D6-DMSO.

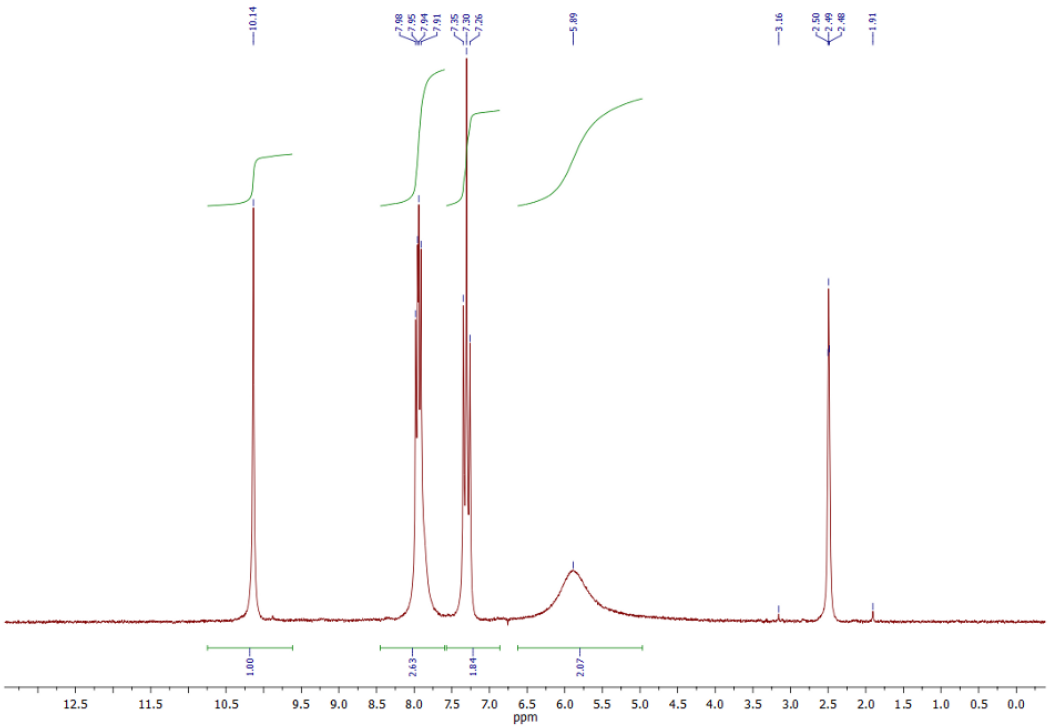

Fig. S20. ^{1}H-NMR spectrum of **4**. Solvent is D6-DMSO.

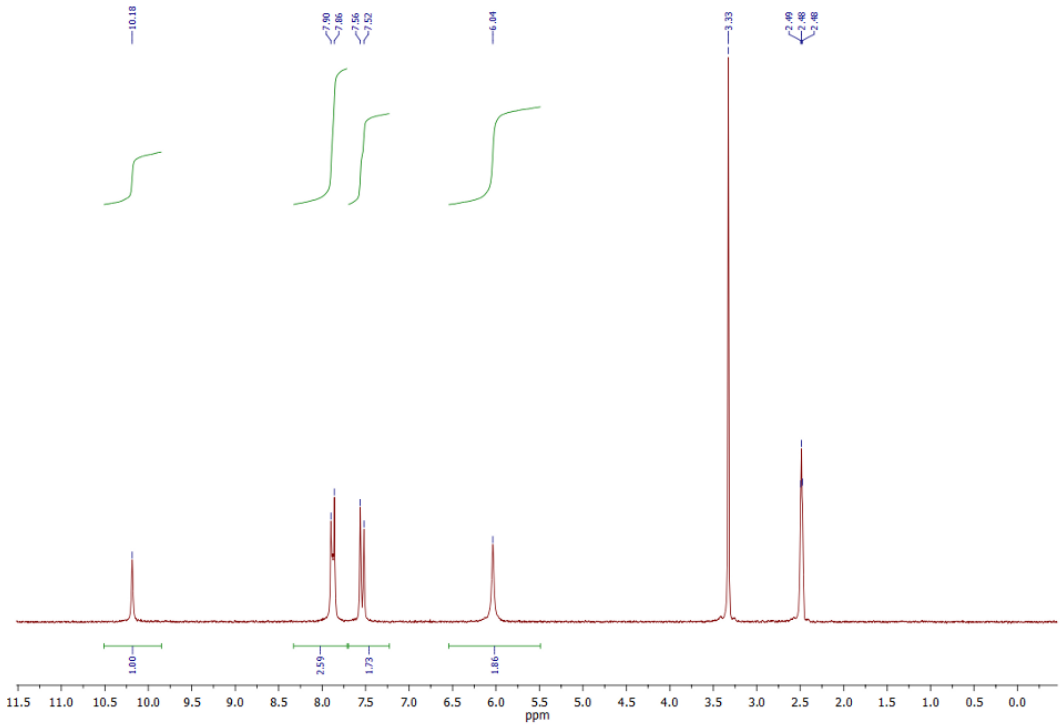

Fig. S21. ^{1}H-NMR spectrum of **5**. Solvent is D6-DMSO.